

Noise Sensitivity-Based Energy Efficient and Robust Adversary Detection in Neural Networks

Rachel Sterneck

Department of Electrical Engineering
Yale University
New Haven, USA
rachel.sterneck@yale.edu

Abhishek Moitra

Department of Electrical Engineering
Yale University
New Haven, USA
abhishek.moitra@yale.edu

Priyadarshini Panda

Department of Electrical Engineering
Yale University
New Haven, USA
priya.panda@yale.edu

Abstract—Neural networks have achieved remarkable performance in computer vision, however they are vulnerable to adversarial examples. Adversarial examples are inputs that have been carefully perturbed to fool classifier networks, while appearing unchanged to humans. Based on prior works on detecting adversaries, we propose a structured methodology of augmenting a deep neural network (DNN) with a detector subnetwork. We use *Adversarial Noise Sensitivity* (ANS), a novel metric for measuring the adversarial gradient contribution of different intermediate layers of a network. Based on the ANS value, we append a detector to the most sensitive layer. In prior works, more complex detectors were added to a DNN, increasing the inference computational cost of the model. In contrast, our structured and strategic addition of a detector to a DNN reduces the complexity of the model while making the overall network adversarially resilient. Through comprehensive white-box and black-box experiments on MNIST, CIFAR-10, and CIFAR-100, we show that our method improves state-of-the-art detector robustness against adversarial examples. Furthermore, we validate the energy efficiency of our proposed adversarial detection methodology through an extensive energy analysis on various hardware scalable CMOS accelerator platforms. We also demonstrate the effects of quantization on our detector-appended networks.

I. INTRODUCTION

Deep neural networks have rapidly accelerated the field of machine learning, demonstrating state-of-the-art performance on a variety of difficult tasks, including computer vision [20], speech recognition [12], and biomedical image analysis [13]. Although neural networks have great potential to be used in real-world vision tasks, their vulnerability to *adversarial attacks* is a bottleneck that must be addressed to ensure that machine learning applications are safe and reliable. Recent research demonstrates that high performing models are vulnerable to small, calculated perturbations applied to images that are capable of fooling a network into misclassifying an input, yet are often imperceptible to humans [6] [11] [14]. In a black-box attack scenario, hackers can create adversarial examples without knowledge of a target model’s parameters by using another network to generate transferable attacks [25]. Furthermore, physical-world adversarial attacks have also fooled classification networks, including printed adversarial examples recaptured with a cell phone camera [3] and stop signs modified with tape perturbations mimicking graffiti [18]. These examples demonstrate the high-risk nature of adversarial

examples, as well as the need to implement defenses against such attacks.

In this paper, we introduce a method for detecting adversarial examples that utilizes the structure of the Convolutional Neural Network (CNN). We use *Adversarial Noise Sensitivity* (ANS) to identify the layers that are most vulnerable to adversarial examples [26]. The idea is to use ANS to determine which layer should be augmented with a detector, improving the robustness of the network in a compute-efficient manner. The detector is a binary classifier trained on intermediate layer activations to distinguish adversarial examples from clean inputs. Intermediate layer activations are obtained from the given layer of the trained CNN onto which one detector is appended. Our results on MNIST, CIFAR-10, and CIFAR-100 empirically show that our method achieves state-of-the-art detection robustness against various adversarial attacks.

To facilitate compatibility with practical hardware accelerators, we quantize the proposed detector-augmented CNN architecture to smaller bit-widths per layer and compare to a 16-bit baseline model. We consider quantized models because network quantization reduces the overall energy consumption of the model by decreasing the number of bits used to represent network parameters, including activations and weights. Given the large number of parameters in a CNN, quantization is a useful method for improving the energy efficiency of accessing and storing DNN parameters without compromising accuracy. We observe that the detector maintains high accuracy even at 1-bit quantization. The quantized CNN with detector network is implemented on a precision scalable hardware accelerator that can support hardware scalability paradigms such as Data Gating (DG) and Dynamic Voltage-Accuracy and Frequency Scaling (DVAFS) [8] [9].

We conduct energy analyses to show that the quantized model consumes considerably less energy than the non-quantized 16-bit CNN and detector model. Furthermore, we demonstrate the energy efficiency of our early adversarial detection scheme by comparing the Multiply and Accumulate (MAC) computation and memory access energies of the standalone CNN network with the quantized detector-appended CNN architecture under various scenarios. We find that the quantized CNN with detector network architecture yields higher energy efficiency than the standalone network for different concentrations of adversarial

examples in the test dataset.

To summarize, we make the following contributions in this paper:

- 1) We improve state-of-the-art detection-based systems for identifying adversarial examples on the CIFAR-10 and CIFAR-100 datasets based on ANS, which allows for a structured addition of detectors to CNNs.
- 2) We demonstrate the energy efficiency of our proposed detector-appended CNN architecture with respect to a standalone CNN network by performing MAC and memory access energy estimation on a precision scalable hardware accelerator with support for DG and DVAFS computation paradigms.

II. BACKGROUND

A. Generating Adversaries

The architecture, parameters, and gradients of a CNN are used to generate adversarial examples. Over the last few years, several methods for creating adversarial examples have been developed, and here we provide an overview of two widely used methods: *Fast Gradient Sign Method* (FGSM) and *Projected Gradient Descent* (PGD).

Fast gradient sign method is a simple method which crafts adversarial examples by linearizing a trained model's loss function (L , e.g. cross-entropy loss) with respect to the input (X) [14]:

$$x_{adv} = x + \varepsilon \text{sgn}(\nabla_x L(\theta, x, y)) \quad (1)$$

Here, y is the true class label for the input image x , θ denotes the model parameters (weights, biases, etc.) ε is the L_∞ -constrained attack strength, and sgn is the sign of the gradient of the loss function. FGSM is not as effective as other algorithms for generating adversaries; however, in our work it provides meaningful insights related to ANS and attack transferability.

Projected gradient descent is regarded as the most effective adversarial attack generated from a network's local first order information, approximately optimizing the perturbations [4]. PGD is an iterative attack that recalculates the gradient and adds perturbations in each iteration:

$$x_{adv}^{t+1} = \Pi_{x+S}(x^t + \alpha \text{sgn}(\nabla_x L(\theta, x, y))) \quad (2)$$

The PGD algorithm is similar to FGSM, however x_{adv}^0 is initialized by adding some random perturbation to the input image, x_{adv}^{t+1} represents the adversarial example of the current iteration, S denotes the set of images in the dataset, and α is the step size in the direction of the sign of the gradient. A key point here is that gradient propagation is a crucial step in adversarial input generation. This implies that the adversarial gradient contribution to the net perturbation ($\text{sgn}(\nabla_x L(\theta, x, y))$) from different layers can vary depending upon the learned activation, which in turn provides the motivation for evaluating the ANS per layer (described more in Section III-A).

B. Hardware Realization

1) **Quantization**: In light of the enormous compute power required by deep learning, quantization is a method of reducing the bit-precision of neural network parameters in order to perform faster and energy efficient computations on large scale hardware accelerators. Recent works have also shown that quantization prevents DNNs from overfitting, and thereby has useful implications, including improved robustness and energy efficiency, without accuracy degradation [26]. Quantization thus serves as a reasonable hardware-centric solution that can be used to realize practical DNN accelerators. Typically, the most common ways of implementing quantization are by using 1) homogeneous bit-precision throughout all layers in the network [16] or 2) mixed-precision, i.e. different layers having different data precision [26].

2) **Hardware Scaling Paradigms**: In terms of DNN accelerator design, parameters such as data and instruction parallelism, voltage of operation, and clock frequency are crucial factors that affect the accelerator performance and energy consumption. One might choose to set the parameters to standard values, which are referred to as the *nominal value*, or use a value lower than *nominal value* called the *scaled value*. In this section, we briefly discuss two hardware scaling paradigms: *Data Gating* (DG) and *Dynamic Voltage-Accuracy and Frequency Scaling* (DVAFS) [8] [9].

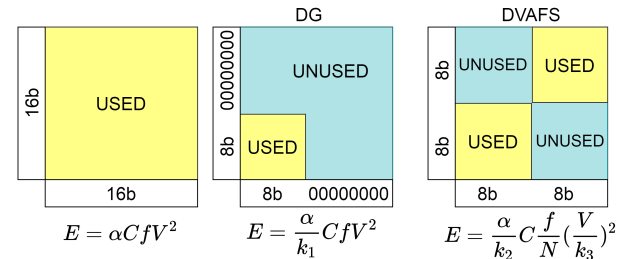


Fig. 1: Comparison of DG and DVAFS hardware scalability paradigms with standard 16-bit MAC computation.

Data gating is a method where the data precision during MAC computation is scaled from the nominal 16-bit precision to a smaller value (i.e. 8-bit) to shorten the critical path of the circuit (which implies faster calculations) such that the supply voltage could be scaled to a lower value. The DG device in Fig. 1 demonstrates that scaling down the voltage V by a factor of k_1 leads to a k_1 times reduction in the consumed energy compared to the standard 16-bit MAC operation. It must be noted that here, the MAC operation occurs between the Most Significant Bits (MSBs) of the input and synaptic weights while the Least Significant Bits (LSBs) are gated, and therefore are not used in the computation which saves energy.

Dynamic voltage-accuracy and frequency scaling is a paradigm shown in Fig. 1 where data-parallelism is implemented at the sub-word level, unlike data-scaling in DG. A sub-word refers to a scaled factor of the maximum word length, for example 2-bit, 4-bit and 8-bit. To illustrate sub-word level

parallelism, let us consider the bit-width of a layer to be 8-bit (which is equal to one of the 3 sub-words mentioned above). In a 16-bit MAC unit, 2×8 -bit (and 4×4 -bit in case of 4-bit sub-word) MAC operations can be performed in parallel. This implies that at the same throughput requirement, $2 \times$ (for 8-bit) and $4 \times$ (for 4-bit) lower frequency, or energy consumption, is required. Also, it can be observed that at sub-word bit-widths, DVAFS utilizes the MAC unit more efficiently than DG [10, 7].

C. Related Work

1) **Adversarial Detection:** Many detection methods have emerged to counter adversarial examples, ranging from augmenting the dataset to modifying the architecture of the network. For example, Goodfellow et al. trained the model on both clean and adversarial examples [14]. Likewise, Grosse et al. used an additional $K + 1$ -th class for identifying adversarial examples [19], and Gong et al. appended a binary classifier to the model that discriminates between real and adversarial inputs [36]. Similarly, Yin et al. developed a method involving input space partitioning and training binary classifiers in subspaces [32]. Most relevant to our work, Metzen et al. appended a binary classifier between convolutional layers to detect intermediate feature representations of an adversary [17]. We consider this to be a more robust approach for detection-based methods because it requires an attacker to not only perturb the input images, but also access and modify the intermediate activations in order to attack the whole system.

Additionally, Bhagoji et al. [5] reduce the dimensionality of the input image fed to the classification network and train a fully-connected neural network on the smaller input. Li and Li [33] build a cascade classifier where each classifier is implemented as a linear SVM acting on the PCA of inner convolutional layers of the classification network. Feinman et al. [29] add a classifier to the final hidden layer of a CNN using a kernel density estimate method to detect the points lying far from the data manifolds in the last hidden layer. However, Carlini and Wagner [24] show that each of these defense methods can be evaded by an adversary targeting that specific defense, i.e. by a white-box adversary.

Likewise, many of the detection methods described above incur a large computational cost and some of them additionally result in an accuracy loss for normal examples. On the contrary, our proposed ANS-based adversarial detection provides a computationally efficient approach for filtering adversaries with high accuracy. By appending the most sensitive layer, i.e. the layer with the highest contribution to adversarial perturbations, with a simple detector, we demonstrate that our method yields strong resilience even against dynamic white-box adversaries wherein both the detector and the network are attacked, as well as black-box attacks involving adversarial examples generated by a substitute model.

2) **Hardware approaches:** Beyond pure algorithmic approaches for minimizing the effects of adversarial attacks, recent works have attempted to solve the problem of adversarial robustness using hardware-algorithm co-design approaches. The authors in [28] show that input data and parameter quantiza-

tion significantly contribute to improvements in adversarial robustness. The paper also shows that *Binary Neural Networks* (BNNs) exhibit higher adversarial robustness than multi-bit precision networks, and the adversarial robustness of BNNs can be further improved by input data quantization. The work on Defensive Quantization (DQ) employs data quantization homogeneously to all the layers of the DNN in order to reduce the error magnification effect in deeper layers by ensuring that the Lipschitz constant value of the network [22] is less than or equal to 1 [15]. Another prominent work is QUANOS [26], which uses mixed precision quantization for different layers in order to introduce robustness during training. This allows the mixed quantized models to perform better than baseline models under FGSM and PGD attacks.

The work by Bhattacharjee et al. [1] discusses the benefits of crossbar non-idealities in light of adversarial robustness. This work shows that device non-idealities in analog crossbars can improve the adversarial robustness by approximately 10-20%. Furthermore, the work on *Conditional Deep Learning* (CDL) by Panda et al. [27] shows that early detection of non-adversarial examples can be very useful in performing energy efficient inference. Here, small linear classifiers are strategically introduced at the end of selected layers to perform early inference. An early-exit approach prevents unnecessary propagation through CNN layers, which in turn saves energy.

In this work, we use early adversarial detection to detect adversarial examples by strategically adding a small binary detector at the end of a specific CNN layer. This facilitates conditional propagation of activation values to deeper layers based on whether the input is classified as clean or adversarial. If the detector classifies the image as adversarial, then its propagation to the later layers is terminated, which prevents unnecessary computations.

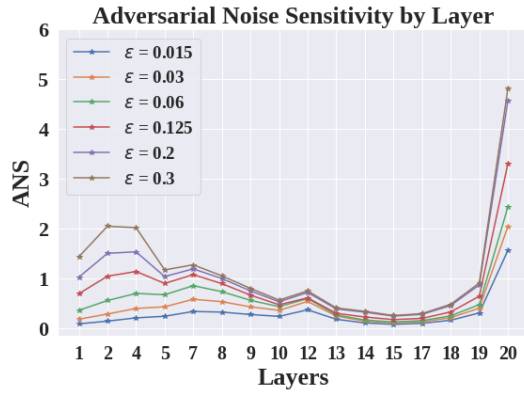
III. METHODOLOGY

A. Adversarial Noise Sensitivity (ANS)

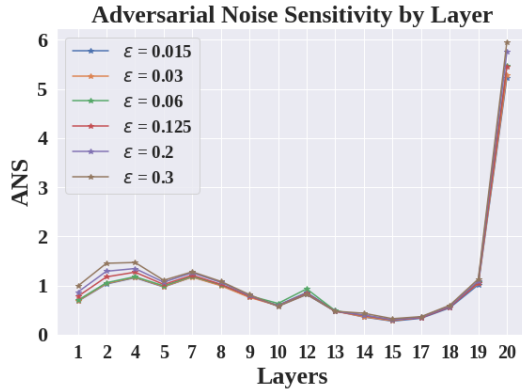
A novel outcome of this work is the application of a new form of noise stability for DNNs, as well as a method for using this metric to evaluate where in the network a detector should be added. ANS provides layer-wise sensitivities to adversarial inputs, and is computed as follows:

$$ANS_l = \sqrt{(a_{adv}^l - a^l)^2} \quad (3)$$

Here, a_{adv}^l and a^l are activation values of layer l when the adversarial input (x_{adv}) and the clean input (x), respectively, are passed through the network. High ANS implies more changes in activations, which can be attributed to high adversarial contribution by a layer. Fig. 2(a),(b) shows ANS for different convolutional layers of a VGG19 model trained on CIFAR-10 data when exposed to FGSM and PGD attacks, respectively. The graphs demonstrate that ANS trends are generally consistent for different attack strengths and types. For example, we identify high ANS peaks at layers 4 and 7 in both Fig. 2(a),(b), even for different FGSM and PGD attacks, which indicates these



(a) ANS for FSGM attacks of varying strength.



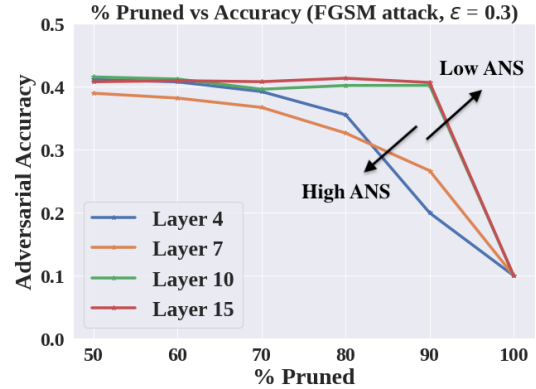
(b) ANS for PGD attacks of varying strength.

Fig. 2: ANS insights for VGG19. The sensitivity trend is similar across different adversarial attacks, and we identify layer 7 as a good detector candidate for detectors trained on low-strength PGD attacks.

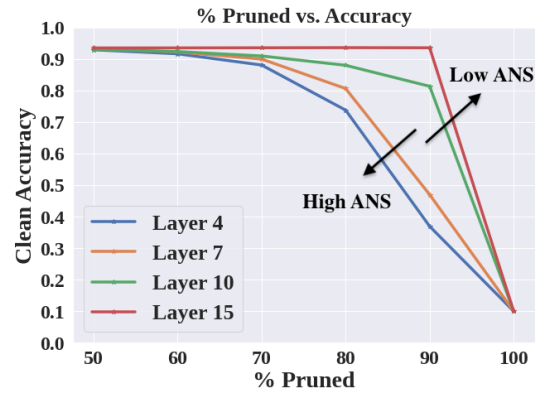
layers are more vulnerable to adversarial attacks than layers with lower ANS values.

To further demonstrate the merit of ANS, we conducted an ablation study that measures the importance of a single direction (i.e. neuronal activations) to a network’s computation by evaluating its performance as the direction is removed. Specifically, we measured the network’s adversarial and clean test accuracies as we pruned the activations of intermediate layers’ neurons, as shown in Fig. 3(a),(b). Fig. 3(a) demonstrates that the decline in adversarial accuracy for high ANS layers is much steeper than that of low ANS layers. This implies that high ANS layers have more important directions and are more susceptible to adversarial attacks. Unless a low ANS layer is completely pruned, its adversarial accuracy is generally unaffected. Furthermore, Fig. 3(b) exhibits that this trend holds for ablation tests on the network with clean examples; again, the low ANS layers decline more gradually, compared to the steep decline of the high ANS layers. This may suggest that high ANS layers generally contribute more to the network overall, even when clean data is passed through. The consistencies between Fig. 2 and Fig. 3 illustrate ANS

as a powerful, yet simple, metric to analyze the contribution of each layer to the net adversarial perturbation during the gradient propagation. That being said, it’s important to note that ANS is a heuristic value, and detector accuracy on a particular layer doesn’t correspond one-to-one with its ANS value. For example, layers 18-20 in Fig. 2(a),(b) have high ANS values, however an ablation test on these deeper layers reveals that their accuracies generally remain unchanged when the convolutional layer is pruned. We believe this happens because later layers predominantly learn high-level features and contribute less to the overall network accuracy than earlier layers that learn more primitive features do [23].



(a) Adversarial accuracy for different amounts of pruning for an FGSM attack with $\epsilon = 0.3$.



(b) Clean accuracy for different amounts of pruning.

Fig. 3: Adversarial Noise Sensitivity (ANS) ablation tests. High ANS layers show a steeper decline in accuracy when pruned.

B. Detector

We use ANS to determine after which layer we must append a detector in the network. Note, we take a trained model and then train the detector separately on the intermediate activations of the trained CNN model. As shown in Fig. 4, we place the detector after a convolutional layer, excluding pooling and fully connected layers as candidates. The detector is a simple binary classifier with two fully connected layers. For our augmented LeNet and VGG19 networks used in Section IV, we create a training dataset of 51,200 samples, and for

ResNet18, we use 25,600 samples; each testing dataset consists of 20,000 activations. Both our testing and training datasets include activations from the corresponding detector layer, and are equally comprised of clean and adversarial activations. Additionally, the detector is trained on a fraction of the original training dataset only, and thus this approach incurs lower training complexity. The detector is trained for a total of 30 epochs, with a learning rate of 0.03 for first 15 epochs and learning rate of 0.003 for the latter 15 epochs.

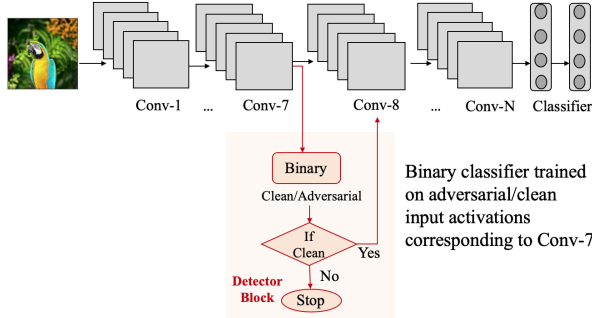


Fig. 4: The network architecture of a VGG19 augmented with an detector.

C. Datasets and Models

In this work, we used PyTorch to train our models and conduct our experiments. For the MNIST [35] dataset evaluations, we used a standard LeNet [34] with 98.6% accuracy trained for 30 epochs with a learning rate of 0.1. The MNIST dataset consists of 60,000 training images and 10,000 testing images. Additionally, for the CIFAR-10 and CIFAR-100 [2], datasets we used VGG19 [21] and ResNet18 [20] models trained for 210 total epochs with a starting learning rate of 0.1 and a learning rate decay of 0.1 at step size 70. The VGG19 network achieves 93.7% accuracy on CIFAR-10 and 70.3% accuracy on CIFAR-100, and the ResNet18 network achieves 95.3% accuracy on CIFAR-10 and 76.7% accuracy on CIFAR-100. The CIFAR-10 and CIFAR-100 datasets consist of 50,000 training images and 10,000 testing images; given the large number of classes relative to the dataset size, CIFAR-100 is regarded as a more difficult classification task. Each model is trained with stochastic gradient descent as the learning algorithm.

D. Robustness Evaluation Metrics

We use Area Under the Receiver Operating Characteristic Curve (AUC) to measure robustness against adversarial attacks. For detection-based approaches geared toward identifying adversarial examples, AUC is a more comprehensive measure than accuracy because it reflects the true positive and false positive rates. The standard accuracy metric assumes that probability scores (softmax outputs) are properly calibrated by imposing a threshold score of 0.5 (i.e. scores above 0.5 are classified as positive and scores equal to or below 0.5 are classified as negative). On the contrary, AUC measures a

classifier’s ability to distinguish between classes, regardless of whether the probability scores are properly calibrated in the range [0, 1]. Intuitively, AUC is the probability that the classifier ranks a randomly chosen positive observation higher than a randomly chosen negative observation [31]. A detector with an AUC score of 1.0 is considered perfect, whereas one with an AUC score of 0 is entirely inaccurate.

Additionally, we consider two robustness tests for white-box attacks: *static white-box* and *dynamic white-box*. In the static white-box case, we assume that the adversary attacks the input images with full knowledge of the CNN’s parameters, but is unaware of the detection mechanism. On the contrary, in a dynamic white-box attack, the attacker has knowledge of the CNN as well as the detector and is capable of perturbing both the images and the intermediate activations. Furthermore, we demonstrate detector robustness against dynamic white-box attacks after we train the detector on dynamic white-box adversaries. We use an approach similar to that of Metzen et al. [17] to train the detector on dynamic white-box adversaries: as we train the detector, we generate PGD attacks on the detector layer’s adversarial activations with 0.5 probability. We consider the dynamic attack all-or-nothing, meaning we either attack both the inputs and activations or neither. It is important to note that the dynamic attack is much more difficult to implement practically, as it additionally requires attackers to modify the neural network internally rather than only provide an adversarial input to the network.

We also simulate black-box attacks on the CIFAR-10 and CIFAR-100 datasets. Similar to the method proposed by Papernot et al. [25] for generating black-box adversarial examples, we train a substitute model to craft adversarial examples that are used to attack the target model. Specifically, in these experiments we use VGG19 substitute models and attack the detector-augmented ResNet18 networks. In our black-box threat model, we assume the adversary has access to the full testing data, however in a real-world scenario it is more likely that an attacker would have to create their own synthetic dataset by observing the output labels for a contrived set of input images.

IV. EXPERIMENTS

A. MNIST

We trained a binary classifier detector on four different attack strengths for both static FGSM and PGD attacks and compare detector robustness between the two attack types. The LeNet implementation we use consists of two convolutional layers followed by two fully connected layers. Here, layer 2 is the high ANS layer, as inferred from a layer-wise ANS graph similar to those in Fig. 2(a),(b). Fig. 5 includes AUC scores for detectors trained and tested at different FGSM and PGD attack strengths. For the FGSM attack, we train and test on attacks with varying epsilon strengths (ϵ), and for the PGD attacks, we train and test on the following parameters: step size (α), attack strength (ϵ), and the number of attack steps (n). The results demonstrate that the LeNet detector is robust against both FGSM and PGD attacks and generally achieves a

greater transferability between different attack strengths when trained on weaker attacks. Comparing the detectors trained on weaker FGSM and PGD attacks, the PGD-trained detector performs slightly better.

		Static FGSM Attack			
		ϵ_{train}			
		0.3	0.5	2.5	5.0
ϵ_{test}	0.3	0.990	0.985	0.693	0.726
	0.5	0.994	0.996	0.761	0.790
	2.5	0.919	0.991	1.000	1.000
	5.0	0.919	0.991	1.000	1.000

		Static PGD Attack			
		Train			
		i	ii	iii	iv
Test	i	1.000	0.980	0.539	0.572
	ii	1.000	1.000	0.599	0.650
	iii	0.980	0.997	0.998	0.995
	iv	0.980	0.997	0.998	0.994

Fig. 5: AUC scores for LeNet with a detector for varying FGSM and PGD attack strengths. The PGD attack labels correspond with the following parameters: **I.** $n = 150$, $\alpha = 0.007$, $\epsilon = 0.125$; **II.** $n = 300$, $\alpha = 0.007$, $\epsilon = 0.125$; **III.** $n = 450$, $\alpha = 0.06$, $\epsilon = 5.0$; **IV.** $n = 600$, $\alpha = 0.06$, $\epsilon = 5.0$.

B. CIFAR-10

Similar to our MNIST experiments, we train a binary classifier on five different PGD attacks, varying in step size (α), attack strength (ϵ), and the number of attack steps (n). We provide results for both VGG19 and ResNet18 neural networks, demonstrating that ANS-based detectors are effective across different CNNs.

1) *VGG19*: We augment our VGG19 network by appending a detector to layer 7 and find that our results are consistent with those on MNIST. Fig. 6 includes AUC scores for detectors trained and tested at different PGD attack strengths for a high ANS layer (layer 7) and a low ANS layer (layer 15). The results demonstrate that a detector placed at a higher ANS layer achieves greater robustness and transferability between attack strengths. Furthermore, with an early-exit strategy for detecting adversarial examples, appending the detector at the end of layer 7 is more energy efficient than augmenting the detector at the end of layer 15. Similar to MNIST, we find the detector is most robust against static PGD attacks when trained on weaker attacks: the detector trained on the PGD attack with $n = 7$, $\alpha = 0.007$, $\epsilon = 0.125$ achieves perfect detectability for a range of PGD attacks.

		Low ANS Detector Robustness (Static PGD Attack)				
		Train				
		i	ii	iii	iv	v
Test	i	0.886	0.849	0.790	0.572	0.571
	ii	0.954	0.992	0.980	0.635	0.651
	iii	0.972	1.000	1.000	0.696	0.709
	iv	0.999	0.997	0.994	1.000	0.998
	v	1.000	1.000	0.999	1.000	1.000

		High ANS Detector Robustness (Static PGD Attack)				
		Train				
		i	ii	iii	iv	v
Test	i	1.000	0.996	0.901	0.743	0.618
	ii	1.000	1.000	1.000	0.963	0.692
	iii	1.000	1.000	1.000	1.000	1.000
	iv	1.000	1.000	1.000	1.000	1.000
	v	1.000	1.000	1.000	1.000	1.000

Fig. 6: AUC scores for VGG19 with a detector attached to low and high ANS layers for varying PGD attacks: **I.** $n = 7$, $\alpha = 0.007$, $\epsilon = 0.125$; **II.** $n = 20$, $\alpha = 0.007$, $\epsilon = 0.125$; **III.** $n = 100$, $\alpha = 0.007$, $\epsilon = 0.125$; **IV.** $n = 40$, $\alpha = 0.5$, $\epsilon = 8.0$; **V.** $n = 200$, $\alpha = 0.5$, $\epsilon = 8.0$.

Furthermore, in Fig. 7 we consider two dynamic attack cases where 1) the detector is trained only on the original activations and 2) the detector is trained on the original activations and attacked activations as described in Section III-D. In the first case, we find that the detector is vulnerable to dynamic attacks on the images and detectors, especially for weaker PGD attacks. In the second case, we demonstrate that we can combat dynamic attacks with high detectability by training the detector on adversarial activations as well. We observe AUC scores of 0 in the dynamic PGD attack cases when the attacks are able to completely fool the detector. Interestingly, we also find that the detectors are able to achieve perfect or near-perfect accuracies for stronger PGD attacks, even in the dynamic attack case. This is likely because the adversarial activations are drastically different from the clean activations to the extent that a PGD activation attack constrained to the L_∞ ball cannot fool the detector.

2) *ResNet18*: In our ResNet18 implementation, we add a detector after the first block (layer 5). We find that our ResNet18 network appended with a detector is able to achieve robustness results on par with our augmented VGG19 network. Furthermore, we demonstrate that the ResNet18-based detection system improves state-of-the-art robustness when trained on a weaker PGD attack. As shown in Fig. 8, the ResNet18 detector trained on weaker PGD attacks achieves AUC scores of 1.0 for the static attacks, and AUC scores of 0.999 and above for the dynamic PGD attacks with training on adversarial activations.

Although we find that detectors trained on stronger PGD attacks are unable to perform well on weaker attacks, this

		Dynamic PGD Attack				
Test	i	0.000	0.000	0.000	0.000	0.000
	ii	0.000	0.000	0.000	0.000	0.000
	iii	0.000	0.000	0.000	0.997	0.994
	iv	1.000	1.000	1.000	1.000	1.000
	v	1.000	1.000	1.000	1.000	1.000
		i	ii	iii	iv	v
		Train				

		Dynamic PGD Attack with Training				
Test	i	0.998	1.000	1.000	0.000	0.000
	ii	0.983	1.000	1.000	0.000	0.000
	iii	0.973	1.000	1.000	0.992	0.996
	iv	0.999	1.000	1.000	1.000	1.000
	v	1.000	1.000	1.000	1.000	1.000
		i	ii	iii	iv	v
		Train				

Fig. 7: AUC scores for VGG19 with a detector for dynamic PGD attacks with and without training on attacked activations: **I.** $n = 7$, $\alpha = 0.007$, $\varepsilon = 0.125$; **II.** $n = 20$, $\alpha = 0.007$, $\varepsilon = 0.125$; **III.** $n = 100$, $\alpha = 0.007$, $\varepsilon = 0.125$; **IV.** $n = 40$, $\alpha = 0.5$, $\varepsilon = 8.0$; **V.** $n = 500$, $\alpha = 0.5$, $\varepsilon = 8.0$.

does not imply that PGD-trained detectors are unable to detect adversarial examples generated by weaker attacks types, such as FGSM. FGSM is considerably weaker than PGD, however Fig. 9 shows that our PGD-trained detector is able to detect FGSM attacks with high discernability, achieving an AUC score of 1.0. Likewise, the FGSM-trained detector also achieves high AUC scores for PGD and FGSM attacks. Additionally, we include detector accuracy to demonstrate that although the FGSM-trained detector tested on PGD-generated adversarial examples is able to distinguish between adversarial and clean examples, it's unable to classify adversarial images when the threshold imposes that the positive class predictions (adversarial examples) corresponds to a probability score greater than 0.5. Follow up analyses reveal that for nearly each test example, the detector classifies the activations as clean because the positive class prediction scores are extremely low. However, there is a stark difference between the positive class probability scores for both the true negative and false negative cases: in the true negative case, about 99% of the positive class probability scores fall in the range $(1e-6, 1e-3]$, and for the false negative case, over 99% of the positive class probability scores fall in the range $(1e-3, 1]$. Thus, if a detector were to use a positive class prediction threshold of 0.001 instead of 0.5 to distinguish between clean and adversarial examples, it would correctly detect adversarial examples with over 99% accuracy.

Additionally, Table I demonstrates that our ResNet18 detector

		Static PGD Attack				
Test	i	1.000	1.000	0.996	0.500	0.500
	ii	1.000	1.000	1.000	0.500	0.500
	iii	1.000	1.000	1.000	0.500	0.632
	iv	1.000	1.000	1.000	1.000	1.000
	v	1.000	1.000	1.000	1.000	1.000
		i	ii	iii	iv	v
		Train				

		Dynamic PGD Attack				
Test	i	0.002	0.000	0.000	0.500	0.500
	ii	0.000	0.000	0.000	0.500	0.500
	iii	0.005	0.000	0.000	0.500	0.500
	iv	1.000	1.000	1.000	1.000	0.770
	v	1.000	1.000	1.000	1.000	0.981
		i	ii	iii	iv	v
		Train				

		Dynamic PGD Attack with Training				
Test	i	0.999	0.995	0.988	0.500	0.475
	ii	1.000	0.997	1.000	0.500	1.000
	iii	1.000	0.800	1.000	0.500	1.000
	iv	1.000	1.000	1.000	1.000	1.000
	v	1.000	1.000	1.000	1.000	1.000
		i	ii	iii	iv	v
		Train				

Fig. 8: AUC scores for ResNet18 with a detector for static and dynamic PGD attacks with the following attack parameters: **I.** $n = 7$, $\alpha = 0.007$, $\varepsilon = 0.125$; **II.** $n = 20$, $\alpha = 0.007$, $\varepsilon = 0.125$; **III.** $n = 40$, $\alpha = 0.5$, $\varepsilon = 8.0$; **IV.** $n = 200$, $\alpha = 0.5$, $\varepsilon = 8.0$.

		Transferability of Attack Types (AUC)	
Test	FGSM	1.000	1.000
	PGD	0.999	1.000
		FGSM	PGD
		Train	

		Transferability of Attack Types (Accuracy)	
Test	FGSM	1.000	0.998
	PGD	0.504	0.998
		FGSM	PGD
		Train	

Fig. 9: Transferability of FGSM and PGD static attacks. The PGD training/testing parameters are $n = 7$, $\alpha = 0.007$, $\varepsilon = 0.125$, and the FGSM training/testing strength is $\varepsilon = 0.3$.

improves state-of-the-art detection on CIFAR-10. Likewise, Table II shows that this detector improves state-of-the-art detectors based on intermediate activations on CIFAR-10. In both comparisons, our ResNet18 detector is trained on a relatively weak PGD attack with $n = 7$, $\alpha = 0.007$, and $\varepsilon = 0.125$.

TABLE I: AUC score comparison with Yin et al. state-of-the-art detector for L_∞ PGD white-box attack [32].

n, α, ε	40, 0.5, 8	200, 0.5, 8
State-of-the-art (Yin et al., 2020)	0.955	0.950
Ours (ResNet18 detector)	1	1

TABLE II: Accuracy comparison with Metzen et al. state-of-the-art intermediate activations-based detector for iterative white-box attack [17].

n, α, ε	10, 1, 2	10, 1, 4
State-of-the-art (Metzen et al., 2017)	0.950	0.960
Ours (ResNet18 detector)	0.998	0.998

Furthermore, we evaluate detector robustness for black-box attack scenarios. Averaging across five trials without a detector, we find that adversarial examples generated from a weak PGD black-box attack ($n = 7$, $\alpha = 0.007$, $\varepsilon = 0.125$) using a VGG19 model degrades the ResNet18 model accuracy to 40.42%; on the contrary, a white-box PGD attack is much more effective, reducing the test accuracy to 0.21%. Additionally we find that a stronger PGD black-box attack ($n = 200$, $\alpha = 0.5$, $\varepsilon = 8$) degrades the model to 10.00%, whereas a white-box attack fools the network entirely, resulting in a test accuracy of 0%. In the case of stronger PGD black-box attacks, we find the minimum attack accuracy to be 10.00% because the ResNet18 model predicts each adversarial example to be the same class. However, once we append a detector to the ResNet18 model, the network is capable of identifying adversarial examples generated from a black-box attack. As shown in Table III, in each of the four black-box attack scenarios tested, the detector is able to perfectly distinguish between adversarial and clean examples, as reflected by an AUC score of 1, and it also classifies adversarial examples with at least 99.7% accuracy. Given the difficulty of identifying black-box adversarial examples, these results further demonstrate the robustness of an ANS-based detector.

C. CIFAR-100

In our ResNet18 implementation for CIFAR-100, we add a detector after the first block (layer 5), finding that our detector is robust against adversarial examples from CIFAR-100. Table IV demonstrates that our ResNet18 detector is robust against static PGD and dynamic PGD attacks, achieving AUC scores of at least 0.999 and 0.991, respectively. To the best

TABLE III: Accuracy and AUC scores for CIFAR-10 black-box attacks on the detector-augmented ResNet18 network. Our detector is trained on a relatively weak L_∞ PGD attack with $n = 7$, $\alpha = 0.007$, and $\varepsilon = 0.125$

n, α, ε	7, 0.007, 0.125	20, 0.007, 0.125	40, 0.5, 8	200, 0.5, 8
Accuracy	0.997	0.998	0.998	0.998
AUC	1	1	1	1

of our knowledge, there is no standard adversarial robustness benchmark on CIFAR-100, however we find that our CIFAR-100 detector performs better than prior detection-based methods do on less complex image classification datasets, including CIFAR-10 (Table I, Table II). These results on CIFAR-100 validate that our ANS-based detector is robust against white-box attacks on more difficult classification tasks.

TABLE IV: AUC scores for CIFAR-100. Our ResNet18 detector is trained on a relatively weak L_∞ PGD attack with $n = 7$, $\alpha = 0.007$, and $\varepsilon = 0.125$. In the dynamic PGD attack, the detector is trained on adversarial activations.

n, α, ε	7, 0.007, 0.125	20, 0.007, 0.125	40, 0.5, 8	200, 0.5, 8
Static PGD	0.999	1	1	1
Dynamic PGD	0.991	0.999	1	1

Consistent with the previous experiments on MNIST and CIFAR-10, we find that detectors trained on weaker PGD attacks are most robust. This occurs due to a one-way transferability with PGD: detectors trained on stronger attacks are more likely to classify adversarial activations from weaker attacks as clean because the training attack strength sets a threshold for adversarial activations, whereas detectors trained on weaker attacks are able to recognize highly-perturbed activations as adversarial because these activations are even more distinct from the clean activations than the training adversarial activations are. Based on our observations, we encourage future research to include transferability results for a range of strong and weak attacks and to consider training on weaker PGD attacks.

Additionally, we consider black-box attack scenarios where adversarial examples are generated from a VGG19 network, and find that the detector-appended ResNet18 network is unable to detect black-box adversarial examples on CIFAR-100. As shown in Table V, the detector performs worse than random in terms of AUC score and accuracy for each adversarial attack scenario tested. This can be explained by the fact that each attack had a false negative rate of about 25% and a false positive rate equal to or close to 100%. Likewise, the results indicate that the detector is unable to distinguish between clean and adversarial examples on the CIFAR-100 dataset. Given the relatively small amount of training data in the CIFAR-100 dataset, it would be worthwhile for future research to investigate the detectability of adversarial examples on other large scale datasets, such as ImageNet.

TABLE V: Accuracy and AUC scores for CIFAR-100 black-box attacks on the detector-augmented ResNet18 network. Our detector is trained on a relatively weak L_∞ PGD attack with $n = 7$, $\alpha = 0.007$, and $\varepsilon = 0.125$

n, α, ε	7, 0.007, 0.125	20, 0.007, 0.125	40, 0.5, 8	200, 0.5, 8
Accuracy	0.430	0.402	0.377	0.377
AUC	0.364	0.252	0	0

D. Quantized Networks

Network quantization compresses the network by reducing the number of bits used to represent the network parameters, including weights and activations. By quantizing a neural network, we can reduce the energy consumption required to access the network weights and to compute and store the activations [30][16]. Here, we explore how we can reduce the data access and computation energies without degrading network robustness against adversarial attacks in the proposed detector-based scheme. Consistent with the earlier experiments, we use a test dataset of 10,000 clean activations and 10,000 adversarial activations from CIFAR-10; the adversarial activations are generated from a PGD attack with $n = 7$, $\alpha = 0.007$, $\varepsilon = 0.125$.

Fig. 10 reflects how the AUC score of the detector changes for varying bit precisions used to represent model weights and activations. We look at three different cases: 1) when only the ResNet18 network parameters are quantized, 2) when only the detector parameters are quantized, and 3) when both the ResNet18 and detector parameters are quantized. When we only quantize parameters for the ResNet18 network, we pass the activations from the quantized network to the detector and find that the AUC score of the detector begins to drop slightly (by 0.001) at a 6-bit precision for ResNet18 and more drastically for 5-bit precisions and below. On the contrary, only quantizing the detector parameters has a negligible effect on the AUC score; the AUC score remains 1.0 for each bit precision shown. Likewise, the AUC degradation trend for quantizing both the ResNet18 and detector parameters is identical to that of the case where only the ResNet18 network is quantized. Due to the fact that the detector robustness is unaffected when the detector is quantized to 1-bit precision, as seen in the second case, the AUC degradation in the third case (when both the ResNet18 model and detector are quantized) can be attributed to the effect of quantization on the ResNet18 network alone. Based on these results, we conclude that we can reduce energy consumption and maintain a strong AUC score by using a 6-bit precision for the ResNet18 and 1-bit precision for the detector. However, before assigning the final bit-precisions for the network and detector, further analysis needs to be performed as explained below.

When evaluating robustness with quantized networks, we must also consider how reduced bit precisions affect the network accuracy for classifying images. Fig. 11 compares changes in ResNet18 network accuracy and detector AUC scores for different bit precisions. We find that although the

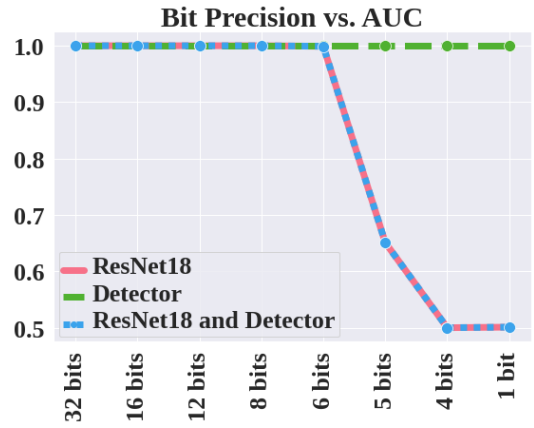


Fig. 10: AUC scores for various bit precisions after quantization of weights and activations for (a) ResNet18 only (b) the detector only and (c) both ResNet18 and the detector.

AUC score degrades for precisions below 6 bits when both the network and detector are quantized, the ResNet18 network accuracy declines for quantized networks smaller than 12 bits. Thus, we use a 12-bit precision for the ResNet18 model and 1-bit precision for the detector in order to maintain the high accuracy as well as robustness of ResNet18.

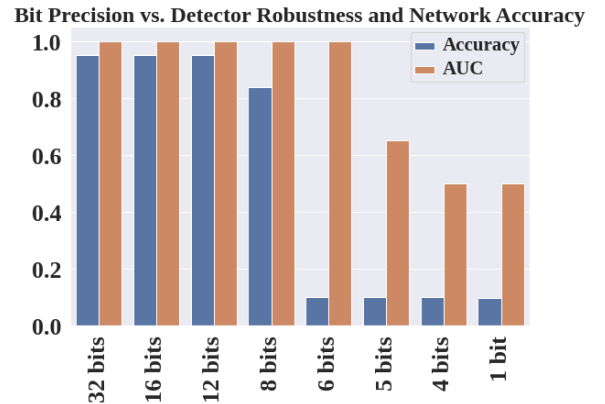


Fig. 11: Detector AUC scores compared to ResNet18 accuracy shown for various bit precisions.

V. HARDWARE IMPLEMENTATION

In this section, we give a detailed explanation of the hardware accelerator implemented for the proposed network-detector architecture described above and additionally demonstrate the energy and compute efficiency of our design under different testing scenarios.

A. Experimental Setup

We design a MAC accelerator shown in Fig. 12 using system verilog descriptions capable of supporting variable data (parameters and activations) precision for each layer. The accelerator can support up to 16-bit data precision. To incorporate hardware scalability, we design the MAC unit to

support DG and DVAFS computation paradigms which enable energy efficient approximate computation [8] [9]. For accurate energy estimations, the design was implemented using 45nm CMOS technology with conservative power models having a nominal supply voltage of 1V. The accelerator can be operated in the following different modes, where $N \in [1,16]$.

- 1) **Basic Mode:** N-bit MAC operations are carried out without employing any hardware scalability methods.
- 2) **DG Mode:** N-bit MAC operations are computed using only MSBs according to the DG convention.
- 3) **DVAFS Mode:** Similar to DG Mode, here MACs are carried out with sub-word level parallelism (of 2X 8-bit and 4X 4-bit levels) and frequency scaling for more energy optimized operations.

The layers in the accelerator are mapped one-to-one with the layers of the proposed model. Each layer has its own parameter memory banks and activation memory banks, along with processing elements (PE) and control circuit (*ctrl_ckt*). Memory banking helps minimize the time and energy required during data-transfer and facilitates parallel implementation. The PE contains the MAC unit that performs MAC operations on the input data. The *ctrl_ckt* serves as the principal component, dictating signals to ensure 1) proper switching between the three modes of operations and 2) accurate data-flow between the memory banks to the processing elements and storage of the activation values.

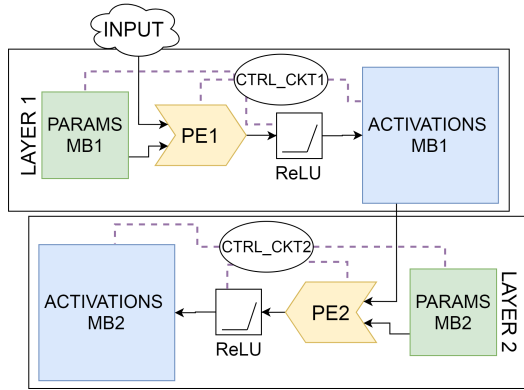


Fig. 12: Block diagram of the hardware accelerator architecture.

B. Energy Analysis

Using the projection of a 45nm CMOS SPICE accelerator implementation, we calculate the energy consumed during a single MAC operation (in all the three modes mentioned previously) and memory access, as shown in Table VI. Here, the energy values provided correspond to 32-bit data memory access and MAC operations. This helps to approximate the energy consumption for any other data precision k_b as mentioned in the Table VI. We will be using these MAC energy values for all our energy analysis experiments.

To evaluate MAC energy in DG and DVAFS paradigms, we vary the data precision in the range [1,16] and obtain the MAC energy per computation. The MAC energy values are

TABLE VI: Energy analysis for single MAC and data-memory access.

Operation	Notation	Energy (pJ)
k_b bit Memory access	E_{A,k_b}	$2.5k_b$
32 bit MULT 32 bit	$E_{M,I}$	3.1
32 bit ADD 32 bit	$E_{Add,I}$	0.1
k_b bit MAC INT	E_{C,k_b}	$(3.1 * k_b) / 32 + 0.1$

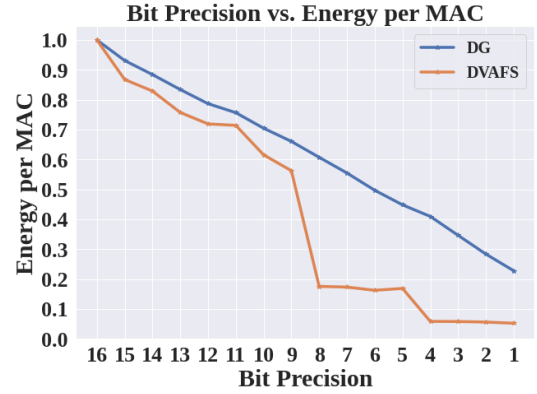


Fig. 13: Normalized energy per MAC against data precision for DG and DVAFS paradigms.

then normalized with respect to MAC energy corresponding to the 16-bit data precision shown in the Fig. 13. We use these normalized values to compare the energy efficiency of our proposed model with baseline models as explained later in this section. In the case of DVAFS for 8-bit and 4-bit precision, it is interesting to note the steep fall in the energy per MAC. This can be attributed to the fact that our accelerator implements $2 \times 8 - bits$ and $4 \times 4 - bits$ sub-word level parallelism for DVAFS. Hence, at 8-bit and 4-bit precision, the frequency (f) can be further decreased to $0.5f$ and $0.25f$, respectively, without affecting the net throughput; this also incurs a larger dip in the energy per MAC.

Typically, energy consumption can be directly related to two major aspects in a DNN accelerator: MAC operation energy and memory access energy. In a convolutional layer, the number of MAC operations is formulated as:

$$N_{MAC} = N_I \times N_O \times M_O^2 \times k^2$$

where N_I is the number of input channels, N_O is the number of output channels, M_O is the output channel size, and k is the kernel size. Likewise, the MAC energy for a layer having k_b -bit data precision can be calculated as:

$$E_{MAC} = N_{MAC} \times E_{C,k_b}$$

To analyze the quantization energy reduction, we compare the MAC energies of homogeneous 16-bit detector-appended network to a 12-bit quantized network with 1-bit quantized detector architecture. At iso-accuracy for clean inputs, the quantized detector-augmented VGG19 network architecture consumes 20% lower MAC computation energy than the 16-bit architecture. Similarly, for ResNet18 architecture, the

quantized network consumes 17% lower MAC computation energy compared to the 16-bit network.

However, the goal of our energy analysis experiments is to demonstrate the energy efficient adversarial example detection capability of our proposed detector-augmented network architecture. For this, we consider a *baseline* model which is the standalone 12-bit quantized main network. The energy efficiency of adversarial detection is shown by subjecting the baseline and proposed detector model to three different testing scenarios: 1) No adversarial inputs 2) 99% adversarial composition, and 3) 1% adversarial composition for the CIFAR-10 dataset. It must be noted that the energy consumed by the *baseline* model will be constant for all three cases because there is no early detection. Since our experiments in Section IV demonstrate that our detector-augmented network is capable of achieving an AUC score of 1 in static and dynamic attack scenarios, we assume that any adversarial example is detected and further propagation is terminated.

Table VII demonstrates the MAC energy efficiency of our approach for the detector-appended ResNet18 network architecture, where the binary detector is placed after the fifth layer of the main network. For the case when there are no adversarial examples, our proposed model consumes slightly more energy when compared to *baseline* because of the detector network overhead. In the case when the concentration of adversarial examples in the test dataset is significant, our model is more energy efficient due to the early-exit. Likewise, there is a greater reduction in energy consumption for larger concentrations of adversarial examples. Using a similar methodology, we perform MAC computation energy analysis on a detector-appended VGG19 network architecture. Here, the detector is placed at the end of the seventh layer. The results are shown in Table VIII.

TABLE VII: MAC Energy results for 12-bit ResNet18 network with 1-bit detector compared with baseline model.

	$E_{MAC,STD}$ (J)	$E_{MAC,DG}$ (J)	$E_{MAC,DVAFS}$ (J)	Reduction
12-bit Baseline	6.93	4.32	3.94	1X
No Adversaries	6.97	4.37	3.96	1.01×
99% Adversaries	2.25	1.42	1.27	0.32×
1% Adversaries	6.92	4.34	3.93	0.99×

TABLE VIII: MAC Energy results for 12-bit VGG19 network with 1-bit detector compared with baseline model.

	$E_{MAC,STD}$ (J)	$E_{MAC,DG}$ (J)	$E_{MAC,DVAFS}$ (J)	Reduction
12-bit Baseline	5.02	3.13	2.86	1X
No Adversaries	5.04	3.14	2.87	1.01×
99% Adversaries	2.44	1.53	1.39	0.49×
1% Adversaries	5.01	3.13	2.84	0.99×

Another important energy contributor is the *memory access energy*. This is the energy cost per access of the memory for read and write operations. The number of memory accesses for a CNN layer can be estimated using the following formula:

$$N_Access_{mem} = N_I \times M_I^2 + N_I \times k^2$$

Using this, we can find the memory access energy E_{mem} , for a layer having k_b bits data precision using,

$$E_{mem} = N_Access_{mem} \times E_{A,k_b}$$

where M_I is the input channel size, E_{A,k_b} is the energy cost per k_b bit memory access, and the other variables follow the previous notation from the MAC operations and energy formulas. Table IX shows the total memory access energy for the 12-bit quantized VGG19 and ResNet18 networks with respective 1-bit quantized detectors attached at the end of the chosen layer. Our findings demonstrate that the memory access energy in the case when the concentration of adversarial examples in the test dataset is 1% is slightly higher than the baseline model, unlike the E_{MAC} case. This can be attributed to the fact that the detector involves about $10\times$ higher number of memory accesses than the number of MAC computations. Finally, to obtain the total energy consumed by the 12-bit CNN with 1-bit detector quantized network, we combine the MAC computation energy and memory access energy values for both the detector-appended VGG19 and ResNet18 network architectures. For simplicity, we only show the energy plots for the detector-appended ResNet18 architecture in Fig. 14.

TABLE IX: Memory access energy results for both ResNet18 and VGG19 networks with detector.

	$E_{mem,ResNet18}$ (J)	$E_{mem,VGG19}$ (J)	Reduction
12-bit Baseline	3.43	3.4	1×
No Adversaries	3.93	3.87	1.14×
99% Adversaries	0.65	0.61	0.18×
1% Adversaries	3.9	3.86	1.13×

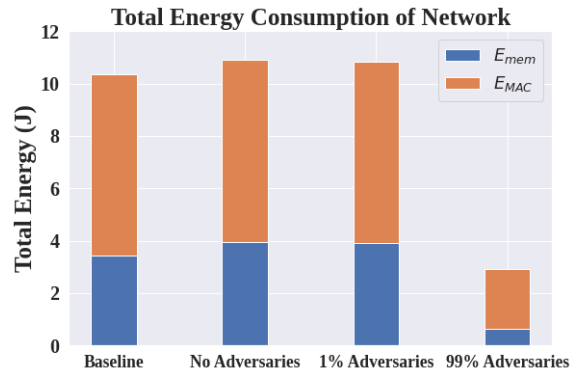


Fig. 14: Total energy consumed by the detector-appended ResNet18 architecture.

VI. CONCLUSION

In this paper, we propose ANS, a novel method for identifying CNN layers that are more sensitive to adversarial attacks based on their intermediate activation features. We demonstrate the value of ANS by using it to develop a detection-based method for identifying adversarial examples.

In this approach, we append a binary classifier, trained on activations, to a layer that is more vulnerable to adversarial attacks. We show that our method improves state-of-the-art results on the CIFAR-10 and CIFAR-100 datasets. To facilitate efficient computing, we analyze the effects of quantization on our detector-augmented network to find the optimal bit-widths for the CNN and detector. Additionally, we perform hardware energy analysis on this quantized model using a precision scalable hardware accelerator to demonstrate that our method not only improves previous methods, but also is more compute efficient than standalone network architectures. We propose ANS-based detectors as a robust and efficient method for preventing adversarial attacks, and we encourage future research to continue analyzing adversarial examples from a structural perspective to help advance the development of safe artificial intelligence.

VII. ACKNOWLEDGEMENT

This work was supported in part by National Science Foundation (Grant No. 1947826), the Technology Innovation Institute, Abu Dhabi and the Amazon Research Award.

REFERENCES

- [1] A. Bhattacharjee et al. Rethinking non-idealities in memristive crossbars for adversarial robustness in neural networks. *arXiv preprint arXiv:2008.11298*, 2020.
- [2] A. Krizhevsky et al. Learning multiple layers of features from tiny images. In *Technical report*, 2009.
- [3] A. Kurakin et al. Adversarial examples in the physical world. *arXiv:1607.02533*, 2016.
- [4] A. Madry et al. Towards deep learning models resistant to adversarial attacks. *arXiv:1706.06083*, 2017.
- [5] A.N. Bhagoji et al. Enhancing robustness of machine learning systems via data transformations. In *2018 52nd Annual CISS*, pages 1–5, 2018.
- [6] B. Biggio et al. Evasion attacks against machine learning at test time. In *ECML PKDD*, 2013.
- [7] B. Moons et al. An energy-efficient precision-scalable convnet processor in 40-nm cmos. *IEEE Journal of solid-state Circuits*, 52(4):903–914, 2016.
- [8] B. Moons et al. Energy-efficient convnets through approximate computing. In *IEEE WACV*, pages 1–8, 2016.
- [9] B. Moons et al. 14.5 envision: A 0.26-to-10tops/w subword-parallel dynamic-voltage-accuracy-frequency-scalable convolutional neural network processor in 28nm fdsoi. In *ISSCC*, pages 246–247, 2017.
- [10] B. Moons et al. Dvafs—dynamic-voltage-accuracy-frequency-scaling applied to scalable convolutional neural network acceleration. In *System-Scenario-based Design Principles and Applications*, pages 99–111. Springer, 2020.
- [11] C. Szegedy et al. Intriguing properties of neural networks. In *ICLR*, 2013.
- [12] D. Amodei et al. . Deep speech 2: End263 to-end speech recognition in english and mandarin. In *ICML*, pages 173–182, 2016.
- [13] D. Shen et al. Deep learning in medical image analysis. In *Annual review of biomedical engineering*, pages 221–248, 2017.
- [14] I.J. Goodfellow et al. Explaining and harnessing adversarial examples. In *ICLR*, 2014.
- [15] J. Lin et al. Defensive quantization: When efficiency meets robustness. *arXiv preprint arXiv:1904.08444*, 2019.
- [16] J. Wu et al. Quantized convolutional neural networks for mobile devices. In *CVPR*, 2016.
- [17] J.H. Metzen et al. Gat: Generative adversarial training for adversarial example detection and robust classification. In *ICLR*, 2017.
- [18] K. Eykholt et al. Robust physical-world attacks on machine learning models. *arXiv:1707.08945*, 2018.
- [19] K. Grosse et al. On the (statistical) detection of adversarial examples. *arXiv preprint arXiv:1702.06280*, 2017.
- [20] K. He et al. Deep residual learning for image recognition. In *CVPR*, 2016.
- [21] K. Simonyan et al. Very deep convolutional networks for large-scale image recognition. In *ICLR*, 2015.
- [22] M. Cisse et al. Parseval networks: Improving robustness to adversarial examples. *arXiv preprint arXiv:1704.08847*, 2017.
- [23] M.D. Zeiler et al. Visualizing and understanding convolutional networks. In *ECCV*, 2014.
- [24] N. Carlini et al. Adversarial examples are not easily detected: Bypassing ten detection methods. In *Proceedings of the 10th ACM Workshop on Artificial Intelligence and Security*, pages 3–14, 2017.
- [25] N. Papernot et al. Practical black-box attacks against deep learning systems using adversarial examples. *arXiv:1602.02697*, 2016a.
- [26] P. Panda. Quanos-adversarial noise sensitivity driven hybrid quantization of neural networks. *arXiv preprint arXiv:2004.11233*, 2020.
- [27] P. Panda et al. Conditional deep learning for energy-efficient and enhanced pattern recognition. In *DATE*, pages 475–480, 2016.
- [28] P. Panda et al. Discretization based solutions for secure machine learning against adversarial attacks. *IEEE Access*, 7:70157–70168, 2019.
- [29] R. Feinman et al. Detecting adversarial samples from artifacts. *arXiv preprint arXiv:1703.00410*, 2017.
- [30] S. Han et al. Deep compression: Compressing deep neural networks with pruning, trained quantization and huffman coding. In *ICLR*, 2016.
- [31] T. Fawcett et al. An introduction to roc analysis. *Pattern Recognition Letters*, 2005.
- [32] X. Yin et al. Gat: Generative adversarial training for adversarial example detection and robust classification. In *ICLR*, 2020.
- [33] X.Li et al. Adversarial examples detection in deep networks with convolutional filter statistics. In *Proceedings*

of the *IEEE ICCV*, pages 5764–5772, 2017.

- [34] Y. LeCun et al. Backpropagation applied to handwritten zip code recognition. In *Neural Computation*, volume 1, pages 541–551, 1989.
- [35] Y. LeCun et al. Gradient-based learning applied to document recognition. In *Proceedings of the IEEE*, 1998.
- [36] Z. Gong et al. Adversarial and clean data are not twins. *arXiv:1704.04960*, 2017.